Inclusive production of K^+ mesons in 2.1-GeV/nucleon nuclear collisions

S. Schnetzer,* R. M. Lombard,† M.-C. Lemaire,† E. Moeller,‡ S. Nagamiya,§ G. Shapiro,**
H. Steiner,** and I. Tanihata††
Nuclear Science Division, Lawrence Berkeley Laboratory, University of California, Berkeley, Berkeley, California 94720
(Received 17 February 1989)

K^+ meson production by 2.1-GeV/nucleon Ne, d, and p projectiles on NaF and Pb targets has been measured. The cross sections depend exponentially upon the kaon energy in the nucleon-nucleon c.m. frame, with an inverse slope T_0 larger than the values obtained from comparable proton and π^- spectra. The angular distribution in this frame is approximately isotropic. The A dependence of the kaon yield has been determined. Data are compared with theoretical predictions.

I. INTRODUCTION

In this paper we report the results of an experiment to measure the inclusive spectra of K^+ mesons produced in collisions of 2.1-GeV/nucleon nuclei with various nuclear targets. The main emphasis will be on proton,, deuteron, and neon projectiles interacting with NaF and Pb targets. The kaons were detected at several laboratory angles between 15° and 80°. They were identified by comparing the momentum measured in a magnetic spectrometer with a time-of-flight measurement, and by observing the kaon decays in an array of Pb-glass blocks. The momentum range of the detected kaons extended from 350 to 750 MeV/c. In the events with the Ne projectile, the associated multiplicity was measured by a set of scintillation counter telescopes, which were situated around the target. Selected features of these data have been presented previously.[1–4] Here we give a detailed description of the experimental apparatus, present all of the cross sections that were measured, and compare our results with various models.

The main interest in relativistic nuclear collisions arises from the fact that these collisions may provide a means of studying nuclear matter under conditions of high density or high temperature. Since the K^+ meson has a relatively long mean free path,[3,4] ≥ 5 fm for $p_K < 1$ GeV/c, it may be a very important probe for studying these conditions. Protons and pions with relatively short mean free paths undergo several collisions and, in the case of pions, may be absorbed and reemitted before they escape from the nuclear material. On the other hand, kaons will have a greater tendency to travel directly from their point of production to the detector and may, therefore, be more reliable harbingers of the early, perhaps highly compressed and hot, stage of the reaction. One of the primary objectives of this experiment was to determine whether the above supposition is indeed correct. A mechanism, for example, which may obscure the information which the kaons carry is their scattering off of the pions produced in the reaction. Because of the K^* resonance these cross sections are quite high.

Another goal of the experiment was to gain insight into the production mechanism of the kaons. In addition to direct kaon production via nucleon-nucleon collisions, $N+N \rightarrow N+Y+K^+$, it is also possible to produce kaons in a two-step process: $N+N \rightarrow \pi+X$ followed by $\pi+N \rightarrow K^++Y$. Although the cross section for the latter is rather high, only pions with momentum greater than about 800 MeV/c are above threshold. This is only a small part of the total pion yield. These two factors, large cross section, and small number of pions which participate, tend to cancel one another with the result that the production of kaons by this mechanism should be comparable to within an order of magnitude to that of the direct NN mechanism. In order to address these questions, we present the data for the various beams and targets and make comparisons with selected theoretical models.[5–27]

Since the completion of this experiment, further K^+ production results have been reported.[17,28–31] The experimental and theoretical situations are well summarized in review articles by Schurmann and Zwermann[12] and Toneev and Gudima,[32] which also contain more extensive references to the theoretical calculations.

The plan of this paper is as follows. In Sec. II we give a detailed description of the experimental setup. In Sec. III the data are presented. We show the differential cross sections as a function of momentum in both the laboratory and nucleon-nucleon center-of-mass frames. We present estimates of the total cross sections and we show the dependence upon the projectile and target masses. In Sec. IV we compare the p-nucleus and Ne-nucleus data with various models. Finally, in Sec. V we summarize the results.

II. EXPERIMENTAL SETUP

The experiment was performed at the Bevalac accelerator of the Lawrence Berkeley Laboratory. Three types of beam particles were used: protons, deuterons, and neon at 2.1 GeV/nucleon. The targets used were C, 1.13 g/cm^2; NaF, 1.20 g/cm^2; KCl, 1.10 g/cm^2; Cu, 0.92 g/cm^2; and Pb, 1.58 g/cm^2. The thicknesses of the targets were chosen to be approximately 1 g/cm^2 in order to provide a sufficient interaction rate while keeping the problem of multiple scattering within the target small.

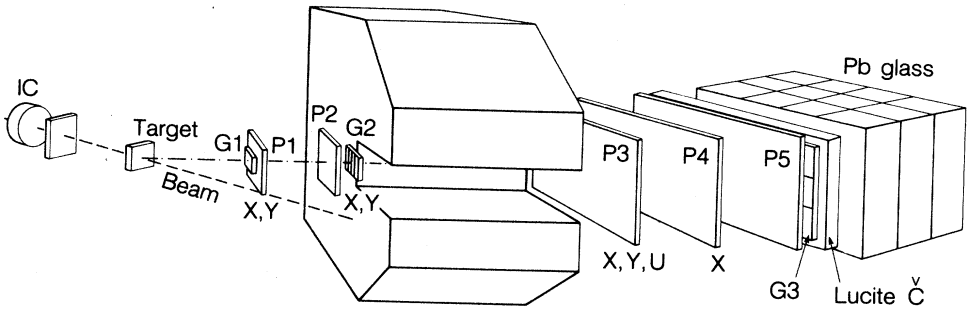

FIG. 1. Sketch of the spectrometer.

An ion chamber 1.5 m upstream from the target was used to monitor the beam intensity. This gave an absolute error in the measured cross sections of 30%.

The spectrometer[33,34] is sketched in Fig. 1 and a vertical plan view is shown in Fig. 2. The geometrical parameters of the various elements of the spectrometer are summarized in Table I. These elements consisted of the following: scintillation counters, bending magnet, wire chambers, Lucite Cerenkov counter, and an array of Pb-glass blocks.

The scintillation counters consisted of the counter $G1$, the five counters $G2(A,B,C,D,E)$, and the three counters $G3(U,C,D)$. All together they served five functions. First, counter $G1$ defined the solid-angle acceptance of the spectrometer for particles emitted from the center of the target. Second, the logic:

$$G1\cdot(G2A+G2B+G2C+G2D+G2E)\cdot(G3U+G3C+G3D)$$

defined the minimum bias trigger, i.e., a charged particle traversing the spectrometer. Third, the time of flight (TOF) between counters $G1$ and $G3$ determined the velocity of the particle traversing the spectrometer. The path length was 210 cm and the full width at half maximum (FWHM) resolution was 500 ps. Fourth, the pulse heights in counters $G1$ and $G3$ allowed charge $=\pm1$ particles to be selected and helped to determine whether there were multiple hits in these counters. Finally the five elements of $G2$, together with the wire chamber $P5$ determined a logic condition matrix which will be discussed later.

The magnet was a standard Bevatron C magnet with a gap spacing of 6 in. and pole tip dimensions of 13 in. $\times$ 24 in. The radius of curvature and thus the particle rigidity, p/Z, was determined by measuring the angle into and out of the magnet. The magnetic field was mapped and was found to be sufficiently uniform so that it could be approximated by a constant field, 6.5 kG, over a volume of 70.4 cm $\times$ 33.0 cm $\times$ 15.2 cm.

The wire chambers $P1$, $P2$, $P3$, $P4$, and $P5$ provided tracking of the particles through the spectrometer, and

TABLE I. Spectrometer elements and wire chamber parameters. For a definition of x, y, and z axes, see Fig. 2.

	Position		Dimension		
Element	x (cm)	z (cm)	x (cm)	y (cm)	z (cm)
C magnet	26.67	165.4	33.0	15.2	61.0
$G1$	8.57	38.35	5.08	3.81	0.64
$G2$ (5 vertical)	17.5	73.81	12.7	7.62	0.32
$G3$ (3 horizontal)	14.0	249.0	55.9	26.7	0.95
Lucite Cerenkov	14.0	254.1	61.0	30.5	5.08
Pb glass	14.0	322.5	60.0	45.0	45.0

	Position		No. of wires		
Wire chamber	x (cm)	z (cm)	x	y	Wire spacing (mm)
$P1$	8.64	41.22	64	64	1
$P2$	14.81	69.16	64	64	2
$P3U$	19.6	167.4	192		2
$P3XY$	19.6	187.3	192	192	2
$P4$	16.74	213.4	256		2
$P5$	16.96	228.6	256		2

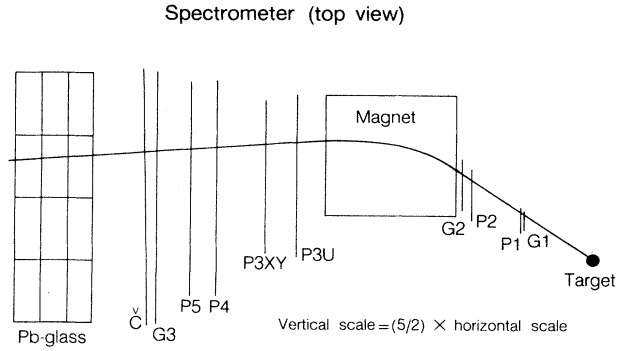

FIG. 2. Vertical view of the spectrometer.

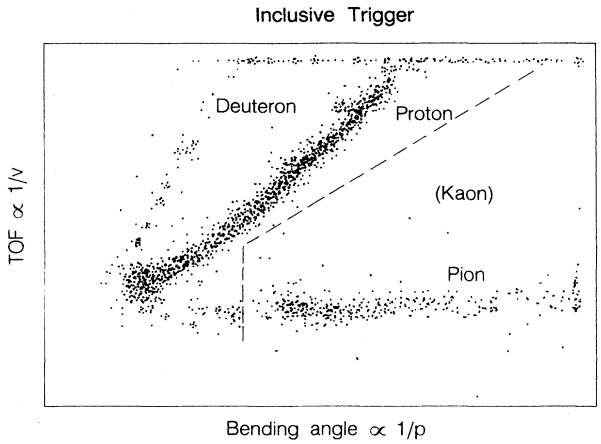

FIG. 3. Scatter plot of TOF vs bending angle for events satisfying the inclusive trigger. Also shown is dashed line indicating the location of the MBD cut.

determined the angles into and out of the magnetic field. Both horizontal and vertical views were provided by $P1$, $P2$, and $P3$, while $P4$ and $P5$ provided only a horizontal view. In addition, $P3$ contained a U plane at 45° for resolving ambiguities.

There were two contributions to the momentum resolution. First, the spatial resolution of the chambers led to some uncertainty in the angles. Second, multiple scattering of the particles, particularly while traversing $G2$, caused the outgoing angle to differ from its value at production. Table II shows the momentum resolution as a function of the momentum as determined by a Monte Carlo simulation taking into account these effects. The resolution, $\Delta(p/p)$, is typically $\pm 10\%$ (FWHM).

A typical plot of time of flight versus bending angle is shown in Fig. 3, where the trigger is $G1 \cdot G2 \cdot G3$, a charged particle traversing the spectrometer. It can be seen that for momenta up to 1 GeV/c the separation between protons and pions is very clean. However, in the region where the kaons should be there are no easily discernible events. This is because the yield of kaons is about 1000 times smaller than that of protons and pions. Thus, in order to acquire satisfactory statistics on kaons we employed a trigger which imposed more stringent criteria. The hardware part of this trigger included a Lucite Cerenkov counter and an array of lead glass blocks.

The Lucite Cerenkov counter was placed downstream of the last wire chamber, $P5$. The light from this counter reached the phototube by total internal reflection at the surface of the counter. Because only light which was internally reflected was detected, particles for which the Cerenkov angle was less than 42° did not produce a signal. The effective threshold β of the counter was 0.84, corresponding to a kaon momentum of 766 MeV/c. This allowed us to reject approximately 99% of the pions above 200 MeV/c and accept 80% of the kaons in the momentum range 350–750 MeV/c.

The lead glass array was used to bring the kaons to a stop and to detect their decay products. The array was 162-g/cm^2 thick, which was sufficient for stopping kaons with momentum up to 750 MeV/c. The K^+ mesons have a proper lifetime of 12.4 ns and decay 65.5% of the time to $\mu\nu$ with $p_\mu = 236$ MeV/c and 30.8% of the time to states containing π^0's. Both of these types of decay created detectable pulses in the lead glass; the μ's produced Cerenkov light directly, while the π's decayed to two γ's which in turn produced electromagnetic showers.

Although the Lucite and lead glass filtered out many of the unwanted particles, high-momentum protons with $\beta > 0.84$ produced Cerenkov light in both the Lucite and lead glass and were accepted. In order to remove these protons two additional trigger elements were used.

Counter $G2$ and chamber $P5$ were divided in the horizontal direction into 5 and 16 sections, respectively. These divisions allowed rough determination of the entrance and exit angles. We set up a matrix logic, MATRIX, to accept only those $G2$ and $P5$ combinations, which could be produced by particles with momentum less than 750 MeV/c. This eliminated some of the high-momentum protons, but an unacceptable number were still accepted. The reason for this was twofold. First, because each $G2$ segment accepted a large range of entrance angles, the position at $P5$ for particles of a particular momentum was very dispersed. Therefore, many particles with momentum greater than 750 MeV/c also satisfied the combination. Second, if there were two particles in the spectrometer, we wished to accept the event if either one was in the acceptable momentum range. There were then a total of four possible $G2$-$P5$ combina-

TABLE II. Momentum resolution.

P (MeV/c)	$\Delta p/p$ resolution due to multiple scattering (%)	$\Delta p/p$ resolution due to wire spacing (%)
300	7.8	2.5
400	6.0	3.8
500	5.0	4.8
600	4.3	6.0
700	3.9	7.1
800	3.6	8.3

tions which had to be accepted.

To reject the remaining protons an on-line software cut based on an MBD (microprogrammable branch driver) was employed. The MBD was able to read the TOF and the $P3X$ and $P5$ wire chamber information before the event was recorded. It could then roughly determine the momentum and, for a given momentum, it would reject those events in which the TOF differed from that of a kaon. The MBD made this decision in about 1 μs.

Applying all of these hardware and software criteria the scatter plot shown in Fig. 3 is changed to that shown in Fig. 4 where the kaons are very clearly seen. During each run data were accumulated with the following four triggers: (1) Inclusive trigger: $G1 \cdot G2 \cdot G3 = G$. (2) Pion trigger: $G \cdot$Lucite. (3) Kaon trigger with MBD cut:

$$G \cdot (\text{Pb glass}) \cdot (\text{Lucite veto}) \cdot \text{MATRIX} \cdot (\text{MBD cut}) .$$

(4) Kaon trigger without MBD cut:

$$G \cdot (\text{Pb glass}) \cdot (\text{Lucite veto}) \cdot \text{MATRIX} .$$

The following two triggers varied from run to run so that the efficiency of the various trigger elements could be determined: (5) Kaon trigger with MBD cut missing one of the following: Lucite veto, Pb glass, MATRIX. (6) Same as (5) but without the MBD cut. All of the above triggers except (4) were prescaled so that the number of events of each type were comparable.

The off-line data analysis took place in four stages: (1) determination of the efficiency corrections, (2) track reconstruction, (3) kaon decay corrections, and (4) determination of the invariant cross sections.

In the first stage, the various acceptances and efficiencies were determined. The geometrical acceptance of the spectrometer was set by the size and position of the scintillation counters, wire chambers, and magnet. This acceptance was calculated by a Monte Carlo program which determined whether particles, which were emitted from the target at various angles and momenta, passed through all of the elements.[33,34] The results are shown in Fig. 5 for particles emitted from the center of the target.

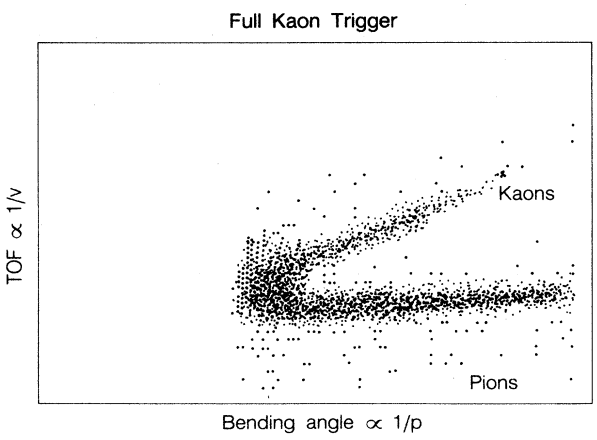

FIG. 4. Scatter plot of TOF vs bending angle for the full kaon trigger.

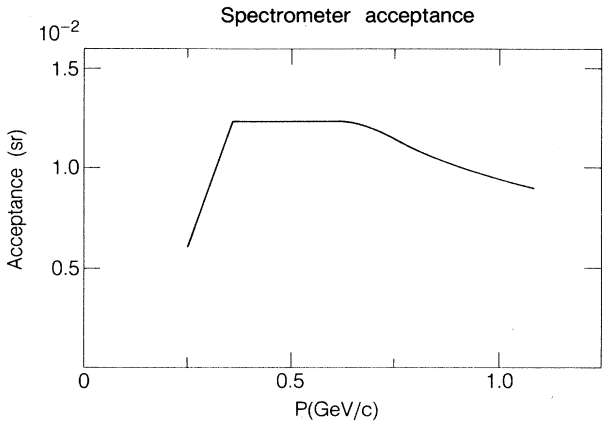

FIG. 5. Acceptance of the spectrometer as a function of momentum.

In addition, there was a dependence upon the source distribution within the target. Therefore, on a run-by-run basis the observed target distribution was determined by extrapolating back to the target using $P1$ and $P2$. The actual target distribution was then determined by dividing by the geometrical acceptance as a function of the target position. This distribution was then input to the Monte Carlo program and the final acceptance was calculated.

Although the wire chambers were not a part of the trigger, they were needed for the off-line tracking. Therefore, if any did not have a hit, the event was rejected. The efficiency of each of the nine planes was determined by requiring that all the other eight planes have hits, and then checking the percentage of events in which the plane in question also recorded a hit. Hits in the other eight planes guaranteed that the particle passed through the plane being tested. The efficiency of each plane was between 97 and 100 %, and the combined efficiency for the nine planes was 80–85 %. Because the overall efficiency varied somewhat from run to run, depending primarily upon the instantaneous rate, this procedure was carried out for each run.

As mentioned above, some runs, in addition to the full trigger, also had a trigger in which a particular element of the full trigger was absent. By checking whether kaons which satisfied the latter trigger also satisfied the full trigger, we could determine the efficiency of the various elements. This was done for the Lucite veto, Pb glass, MATRIX, and MBD cut. The efficiencies of the Lucite veto and Pb glass are shown in Figs. 6 and 7. The efficiencies of the MATRIX and MBD cut were 100%.

In order to select real particle tracks, we required that the following four criteria be fulfilled: (1) Using the information in $P1$ and $P2$, the track should extrapolate to the center of the target. (2) The horizontal trajectories determined by $P3X$ and $P5$ and by $P1X$ and $P2X$ should cross at the center line of the magnet. (3) The vertical trajectories determined by $P3Y$ and $P2Y$ and by $P2Y$ and $P1Y$ should have the same slope. (4) The 45° $P3U$ coordinate should be consistent with the $P3X$ and $P3Y$ coordinates.

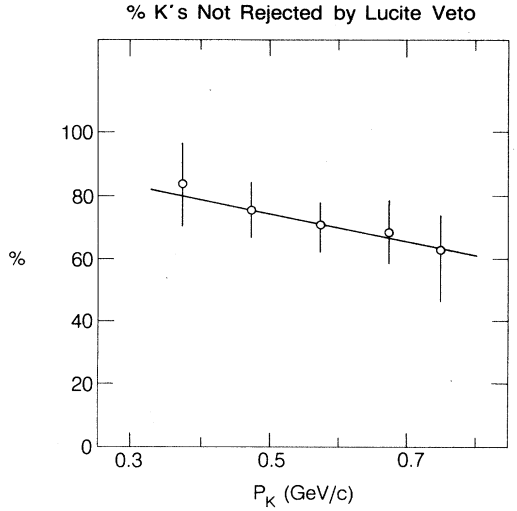

FIG. 6. Percentage of kaons accepted by the Lucite counter veto as a function of kaon momentum.

Using these criteria, we were able to reject enough spurious tracks so that clean particle separation could be made and so that the background was sufficiently small.

Since kaons have a proper lifetime of 12.4 ns, the number that decay before reaching $G3$ which is 249 cm from the target represents an important correction. Table III shows this correction as a function of the kaon momentum. One possible complication is that the μ from the K decay may make it through the system and mimic the kaon. This problem was studied using Monte Carlo techniques and was found to be less than a 1–2 % correction.

Table IV summarizes the corrections made to the data and the associated errors. These are separated into those which have little or no momentum dependence and those which do depend upon the momentum. The overall absolute error is $\approx 30\%$. The relative errors for the cross sections at different values of momentum are less than 10%.

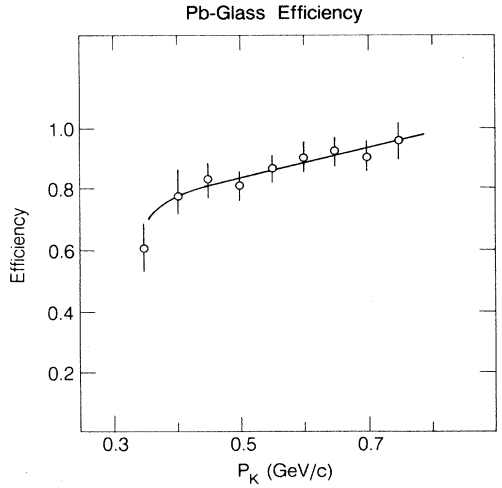

FIG. 7. Pb-glass efficiency as a function of the kaon momentum.

TABLE III. Corrections for kaon decay in flight.

Momentum	Correction factor[a] f
350	0.38
400	0.43
450	0.47
500	0.51
550	0.54
600	0.57
650	0.60
700	0.62
750	0.64

[a]Correction factor defined by $f \equiv N_{\text{det}}/N_{\text{true}} = e^{-L/\beta\gamma ct}$, where L is the distance the kaon must travel in order to be detected, βc is the kaon velocity, and γt is the Lorentz dilated lifetime.

III. RESULTS

A. Kaon spectra

In this section, we present the spectra of the invariant differential cross sections for K^+ production on NaF and Pb targets for all laboratory angles, which were measured and for all three-beam particles: protons, deuterons, and Ne. Figures 8–13 show these spectra as functions of the laboratory kaon momentum. The values of the cross sections are given in Table V.

In the laboratory frame, the spectra for all of the target-projectile combinations are qualitatively very similar. For each projectile-target combination, the cross section decreases with increasing laboratory angle, and the slopes of the spectra become steeper with increasing laboratory angle. For a given projectile, both of these angular dependences are less for the Pb target than for the NaF one.

The kinematical region that these measurements cover is shown in Fig. 14, where the measured points are plot-

TABLE IV. Efficiency corrections and errors. Correction value is defined as the percent of the events lost due to the specified item.

Type of correction	Correction to cross section (%)	Error[a] in cross section (%)
Absolute beam intensity	0	5
Dead time	30	1
MWPC efficiency	20	10
Track reconstruction	25	10
dE/dx scatter plot cut	10	3
Decay in flight	30	1
Spectrometer acceptance	0	5
Pb-glass efficiency	15	15
AntiLucite efficiency	30	15
Total		30

[a]Error in percent of cross section, not in percent of correction.

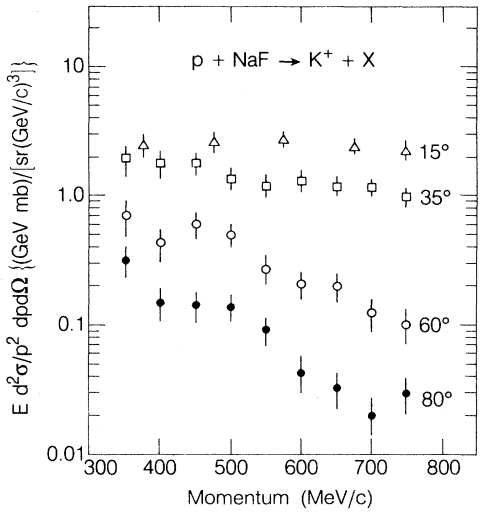

FIG. 8. Invariant cross section for $p+\mathrm{NaF}\rightarrow K^+X$ vs K^+ momentum for lab angles of 15°, 35°, 60°, and 80°.

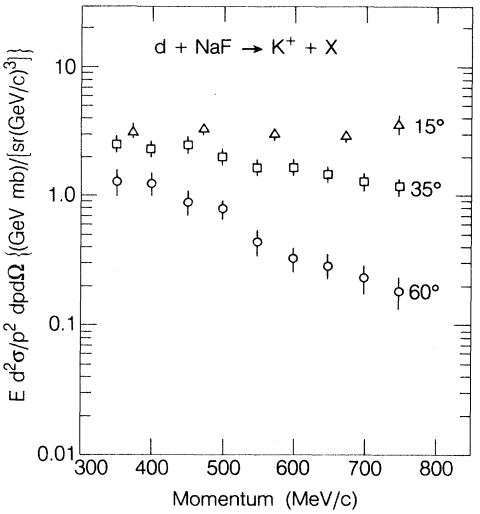

FIG. 10. Invariant cross section for $d+\mathrm{NaF}\rightarrow K^+X$ vs K^+ momentum for lab angles of 15°, 35°, and 60°.

ted on a rapidity-P_T plot. It is important to note that the kinematical region covered by this experiment is very limited. This must lead to caution when trying to draw conclusions about the general nature of the K^+ yield such as, the values of the total cross sections and the degree of angular isotropy. In addition, the data at different values of P_T are, in general, also at different values of the rapidity, with larger values of P_T weighted more toward the target rapidity. Also shown in this figure are the kinematical limits on kaon production for free-nucleon-nucleon collisions, and for collisions of two nucleons each with 270 MeV/c of Fermi momentum. All of the 55° and 80° data are beyond the free-nucleon-nucleon limit, and the last point at 80° is beyond the 270 MeV/c Fermi momentum limit. Clearly, some nuclear effects are required in order to explain the data.

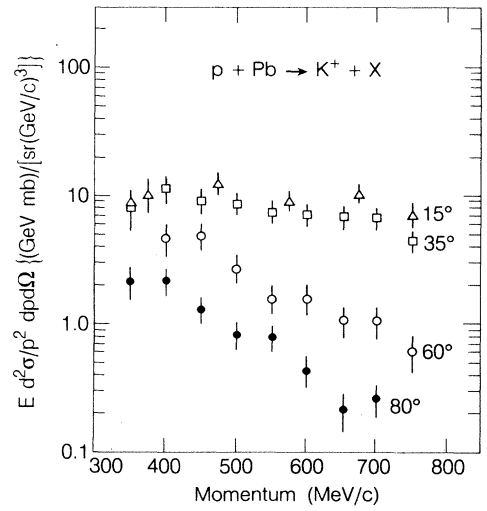

FIG. 9. Invariant cross section for $p+\mathrm{Pb}\rightarrow K^+X$ vs K^+ momentum for lab angles of 15°, 35°, 60°, and 80°.

In Fig. 15, we plot the cross sections for three sets of data: Ne+Pb, Ne+NaF, and p+Na vs T^*, the kaon kinetic energy in the NN c.m. system. For each of the three target-projectile combinations, the data tend to lie on exponential curves.

B. Total cross sections

In this section, we use the plot in Fig. 15 to estimate the values of the total cross section for K^+ production. Since the data cover a very limited kinematical region, it is very difficult to obtain a precise value for the total cross section. However, we can obtain a reasonable estimate by using the approximate isotropic and exponential behavior of the data in the nucleon-nucleon center of mass. We integrate over the center-of-mass energy by extrapolating the exponential dependence and we integrate over angles by assuming isotropy. By this method, we

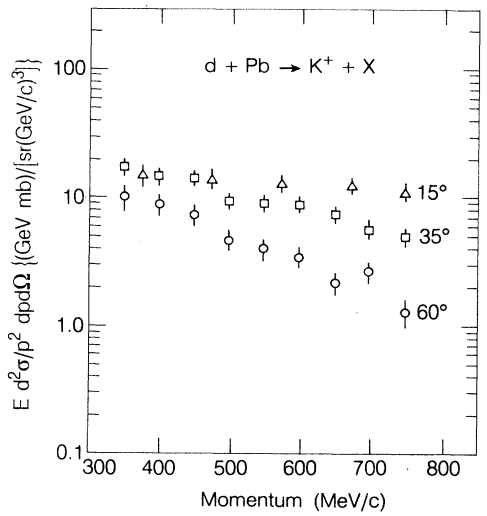

FIG. 11. Invariant cross section for $d+\mathrm{Pb}\rightarrow K^+X$ vs K^+ momentum for lab angles of 15°, 35°, and 60°.

TABLE V. Invariant cross sections.

Momentum (MeV/c)	$\theta_L=15°$	$\frac{Ed^2\sigma}{p^2dp\,d\Omega}\left[\frac{\text{GeV mb}}{\text{sr (GeV}/c)^3}\right]$ $\theta_L=35°$	$\theta_L=60°$	$\theta_L=80°$
		p + NaF		
350	3.2±0.8	1.9±0.5	0.70±0.22	0.31±0.08
400	2.3±0.5	1.8±0.4	0.43±0.13	0.14±0.04
450	2.7±0.5	1.8±0.3	0.60±0.13	0.14±0.03
500	2.7±0.4	1.4±0.2	0.50±0.10	0.14±0.03
550	2.8±0.4	1.2±0.2	0.27±0.07	0.09±0.02
600	2.8±0.4	1.4±0.2	0.21±0.05	0.04±0.01
650	2.3±0.3	1.2±0.2	0.20±0.05	0.03±0.01
700	2.9±0.4	1.2±0.2	0.12±0.03	0.02±0.01
750	2.3±0.3	1.0±0.2	0.10±0.03	0.03±0.01
		p + Pb		
350	9±5	8.5±3.0	9.0±2.2	2.5±0.6
400	12±4	11.7±2.8	4.8±1.2	2.5±0.5
450	15±4	9.6±2.1	5.0±1.0	1.3±0.3
500	9±2	9.0±1.7	2.9±0.7	0.87±0.2
550	9±2	7.8±1.5	1.6±0.4	0.82±0.2
600	9±2	7.4±1.3	1.6±0.4	0.45±0.1
650	10±2	7.1±1.2	1.1±0.3	0.22±0.1
700	11±2	6.9±1.2	1.1±0.3	0.27±0.1
750	7±2	4.3±0.8	0.6±0.2	0.07±0.03

Momentum (MeV/c)	$\theta_L=15°$	$\frac{Ed^2\sigma}{p^2dp\,d\Omega}\left[\frac{\text{GeV mb}}{\text{sr (GeV}/c)^3}\right]$ $\theta_L=25°$	$\theta_L=35°$	$\theta_L=60°$
		d + NaF		
350	2.7±0.6	2.5±0.5	2.0±0.4	1.08±0.30
400	2.6±0.5	3.3±0.5	2.2±0.3	1.26±0.26
450	3.1±0.5	3.3±0.4	2.4±0.3	0.89±0.18
500	3.6±0.5	3.1±0.4	2.0±0.3	0.78±0.14
550	3.2±0.4	2.9±0.4	1.6±0.2	0.44±0.09
600	2.9±0.4	2.7±0.3	1.7±0.2	0.31±0.07
650	3.3±0.4	2.8±0.3	1.5±0.2	0.29±0.06
700	2.8±0.3	2.5±0.3	1.2±0.2	0.23±0.05
750	3.7±0.4	2.1±0.2	1.1±0.1	0.18±0.04

Momentum (MeV/c)	$\theta_L=15°$	$\frac{Ed^2\sigma}{p^2dp\,d\Omega}\left[\frac{\text{GeV mb}}{\text{sr (GeV}/c)^3}\right]$ $\theta_L=25°$	$\theta_L=35°$	$\theta_L=80°$
		d + Pb		
350	11±3	18±3	15.7±2.5	8.6±2.2
400	17±3	16±3	14.9±2.0	8.9±1.8
450	15±2	13±2	14.0±1.8	7.3±1.3
500	13±2	14±2	9.4±1.2	4.7±0.9
550	13±2	11±1	9.0±1.1	4.0±0.8
600	13±2	13±2	9.0±1.1	3.5±0.6
650	12±2	9±1	7.5±0.9	2.2±0.5
700	13±2	9±1	5.8±0.7	2.8±0.5
750	11±1	9±1	5.0±0.6	1.3±0.3

Momentum (MeV/c)	$\theta_L=15°$	$\theta_L=25°$	$\frac{Ed^2\sigma}{p^2dp\,d\Omega}\left[\frac{\text{GeV mb}}{\text{sr (GeV}/c)^3}\right]$ $\theta_L=35°$	$\theta_L=45°$	$\theta_L=55°$	$\theta_l=80°$
			Ne + NaF			
350	26±5	26±4	22±3	19.9±3.9	11.6±1.9	3.28±0.60
400	24±4	30±4	21±3	15.0±2.7	8.7±1.3	3.20±0.49

TABLE V. (*Continued*).

Momentum (MeV/c)	$\theta_L=15°$	$\theta_L=25°$	$\theta_L=35°$	$\theta_L=45°$	$\theta_L=55°$	$\theta_l=80°$
			$\frac{Ed^2\sigma}{p^2dp\,d\Omega}\left[\frac{\text{GeV mb}}{\text{sr (GeV}/c)^3}\right]$			
			Ne+NaF			
450	23±4	24±3	21±2	12.2±2.0	7.3±1.1	1.90±0.30
500	29±3	29±3	21±2	13.8±2.0	7.1±1.0	1.50±0.23
550	24±4	24±3	18±2	10.5±1.6	4.8±0.7	1.03±0.17
600	31±3	23±3	18±2	8.6±1.3	4.9±0.7	0.97±0.15
650	25±3	21±2	14±2	8.4±1.2	3.4±0.5	0.71±0.12
700	25±3	21±2	13±1	6.7±1.0	3.4±0.5	0.55±0.10
750	30±4	20±2	13±1	6.6±1.0	2.7±0.4	0.37±0.07
			Ne+Pb			
350	253±57	153±29	251±38	146±24	128±22	58±9
400	186±38	210±30	166±24	116±17	102±16	40±6
450	193±34	210±28	153±20	117±16	90±13	32±5
500	202±32	171±22	126±16	90±12	76±11	24±3
550	168±26	156±20	135±17	86±11	64±9	17±3
600	201±28	159±19	129±16	74±9	64±9	16±2
650	169±24	135±16	112±14	63±8	43±6	11±2
700	162±23	137±16	107±13	68±8	43±6	15±2
750	197±26	133±16	83±10	78±9	44±6	7±1

obtain the values for the cross sections given in Table VI.[4] Obviously these values are very approximate. First the extrapolation process itself contributes a large fraction to the quoted error. This is the error given with the above values in Table VI. In addition, if there is even a slight amount of anisotropy, for example, some forward-backward peaking, then the error will become much larger. The approximation of isotropy is, of course, not as good for the cases of unequal target-projectile masses. Therefore, the value for Ne+NaF is probably the most reliable.

C. *A* dependence

In order to determine the dependence of the kaon yield on the mass of the target, we integrate each of the measured spectra over the momentum range of 350–750 MeV/c for each angle. We, thereby, obtain $d\sigma/d\Omega$ for laboratory angles of 15°, 25°, 35°, 45°, 55°, and 80°. At 25° and 55° a total of five targets were used; C, NaF, KCl, Cu, and Pb, while at the other angles only data for NaF and Pb are available. Figure 16 shows the results for Ne projectiles on the various targets. From this figure we see that the dependence on the target mass number, A_T in-

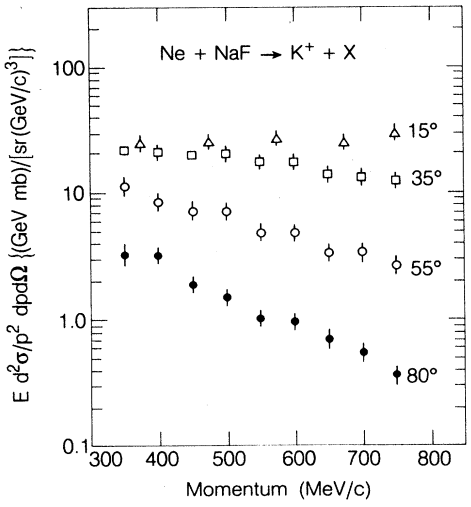

FIG. 12. Invariant cross section for Ne+NaF→K^+X vs K^+ momentum for lab angles of 15°, 35°, 55°, and 80°.

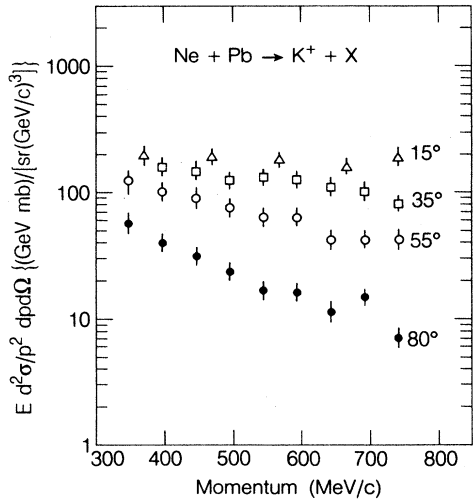

FIG. 13. Invariant cross section for Ne+Pb→K^+X vs K^+ momentum for lab angles of 15°, 35°, 55°, and 80°.

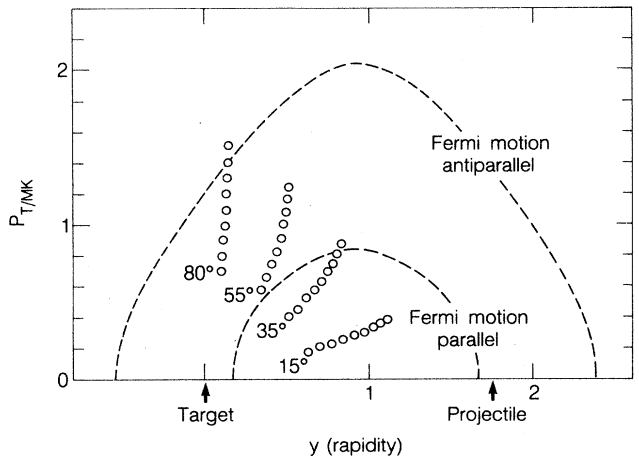

FIG. 14. Plot of transverse momentum P_T/m_k of the emitted particle as a function of rapidity $y=\frac{1}{2}\ln[(E+P_\parallel)/(E-P_\parallel)]$ showing the kinematical region covered by this experiment (circles). Dashed curves indicate the kinematical limit with a maximum Fermi momentum of 270 MeV/c parallel and antiparallel to the motion of the nucleon.

creases with increasing laboratory angle. In an A_T^α parametrization, α varies from smaller than 1 for angles less than 45° to greater than 1 for angles larger than 55°. In Fig. 15 the cross sections, $(d^2\sigma/p^2dp\,d\Omega)$, are plotted versus kaon center-of-mass energy T^*. The Ne+Pb points are typically about an order of magnitude higher

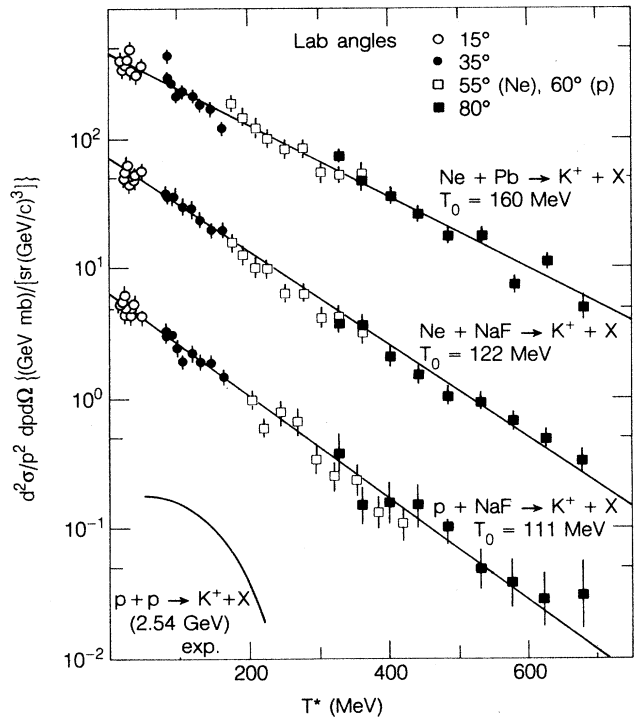

FIG. 15. Cross section $d\sigma^2/p^2dp\,d\Omega$ vs kinetic energy of K^+ in the nucleon-nucleon c.m. frame for Ne+Pb$\rightarrow K^+X$, Ne+NaF$\rightarrow K^+X$, and p+NaF$\rightarrow K^+X$. The data of Ref. 38 are indicated by a full curve. The lines passing through the points are drawn to guide the eye.

TABLE VI. Values of the total cross section for K^+ production.

Reaction	σ_{tot} (mb)
p+NaF	1.8±0.6
p+Pb	11±4
d+NaF	2.4±0.8
d+Pb	14±5
Ne+NaF	23±8
Ne+Pb	150±90

than those for Ne+NaF. The inverse slope factor, T_0, defined by

$$\frac{d^2\sigma}{p^2dp\,d\Omega}\propto\exp(-T^*/T_0)\ ,$$

is 160 MeV for Ne+Pb collisions, and 122 MeV for Ne+NaF. Corresponding results for pion production in Ne+"A" collisions show a similar trend, but with an even steeper fall off with T^* (95 MeV vs 85 MeV),[33,35,36] presumably due to the higher probability for rescattering.

With respect to projectile mass dependence, we note that at small angles the ratio of cross sections with a deuteron to those with a proton projectile is only 1.3±0.2. This is consistent with the fact that production of positive kaons by neutrons is less likely than that by protons. An evaluation[4] of the ratio $\sigma(d+\text{NaF})\rightarrow K^+X$ to $\sigma(p+\text{NaF})\rightarrow K^+X$ using one-pion-exchange model and the procedure of Ref. 5 to estimate the values of the basic NN cross sections for K^+ production[37] gives a value

$$\frac{\sigma(d+\text{NaF}\rightarrow K^+X)}{\sigma(p+\text{NaF}\rightarrow K^+X)}=1.6\pm0.1$$

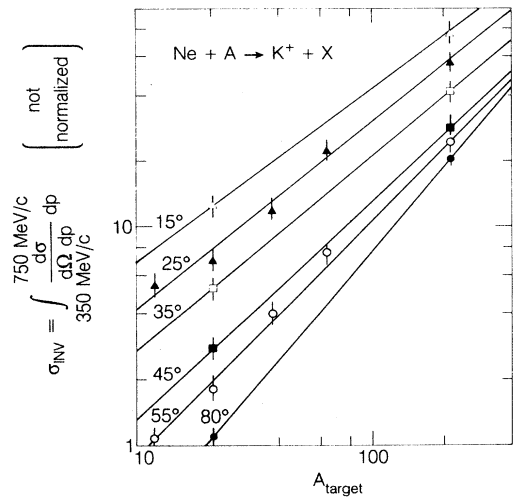

FIG. 16. $\sigma_{inv}=\int_{350\ MeV/c}^{750\ MeV/c}d\sigma/(dp\,d\Omega)dp$ as a function of A for Ne+$A\rightarrow K^+X$ at angles of 15°, 25°, 35°, 45°, 55°, and 80°. The full lines are drawn to guide the eye.

IV. DISCUSSION OF THE NUCLEON-NUCLEUS AND NUCLEUS-NUCLEUS DATA

In this section we will discuss the main features of the data and compare our measurements with various theoretical models.[5-27] Our most important conclusion is that no unconventional or exotic mechanisms need to be invoked to explain our observations. Both intranuclear cascade type calculations and thermodynamic models have been refined enough in recent years to describe our results. In fact we will show that the essential features of the data can even be reproduced with two very naive models—one based on individual nucleon-nucleon collisions including Fermi motion, the other involving collisions between small clusters of nucleons.

An important difference between K^+ production in p-nucleus (or nucleus-nucleus) collisions and in free-p-p collisions is kinematic; i.e., at any given bombarding energy per nucleon there is more phase space available to the kaon when nuclei are involved. This can be seen in Fig. 15 where we have plotted the cross section for p-p collisions at 2.54 GeV.[38] It falls off sharply with kaon energy, going to zero at the maximum energy which is kinematically allowed. In contrast the kaon spectrum in p-nucleus collisions falls off much more slowly with energy, and extends well above the free-nucleon-nucleon limit. When plotted as a function of energy in the nucleon-nucleon center of mass these cross sections show an exponential dependence out to the largest kaon energies measured.

A related feature is the fact that the kaon spectra produced in p-nucleus and nucleus-nucleus collisions have similar shapes. In all of these cases the cross sections fall exponentially with kaon energy, although the falloff with energy is slightly less steep for nuclear projectiles. This behavior is also expected simply on the basis of the kinematics.

The exponential dependence of the cross sections in the nucleon-nucleon c.m. frame indicates that there is some degree of isotropy in this frame. However, it should be kept in mind that our measurements extend only over a very limited kinematic domain, so that one should not draw too strong a conclusion from this. In p-nucleus collisions the target nucleus is the only source of the extra energy needed to produce kaons with energies greater than the maximum energy allowed in free-nucleon-nucleon kinematics. Thus the source of these kaons must be biased toward the target rapidity. On the other hand the isotropy of the low-energy kaons is expected if reactions of the type $NN \rightarrow YNK$ play an important role. Here N is either a proton or a neutron and Y is either a Λ or Σ hyperon.

We turn now to a discussion of the various models which have been used to describe our results. As in other high-energy nucleus-nucleus reactions these fall into two general classes—microscopic and macroscopic. The intranuclear cascade is the typical example of the first class, whereas the thermodynamic model exemplifies the second. Both have been used with varying success in describing particle production, and application to the present experiment provides yet another testing ground. It is not surprising that as more and more of the basic physics is incorporated into these models, and as the experimental conditions more and more closely approximate the underlying assumptions of these approaches, the agreement with the data improves. Thus we do not see the various models in competition in the sense that one of them should ultimately prevail, but rather as attempts to find relatively simple approximations to rather complicated multiparticle interactions. In fact the approximations inherent in these calculations often apply better to certain kinematical regions of a given reaction than to others, so that in the absence of a complete theory a combination of models may sometimes be needed to get the desired agreement with all of the observations.

A. Microscopic models

In the microscopic models to be considered here the dominant K^+ production mechanism is assumed to be $NN \rightarrow YNK^+$. Whenever possible, existing data are used as input, but unfortunately these are not available in many cases so that interpolations, extrapolations, and sometimes even more questionable assumptions have to be made, all of which limit the reliability of the results. For example, in the two simple calculations which we have performed, and which we will describe shortly, we use data obtained in p-p collisions at 2.54 GeV (Ref. 38) to estimate the basic cross sections at the energy of our experiment, 2.1 GeV. To do this we note that the data at 2.54 GeV are best fit by assuming 60% Σ and 40% Λ production, and that the kaon spectra are well described by assuming that all of the available phase space is uniformly occupied. Because 2.1 GeV is closer to threshold we assume a 50-50 % mix of lambdas and sigmas, and that the dependence of the kaon production cross section on center-of-mass energy is determined by the total available phase space. The phase space available is approximately proportional to the maximum momentum of the lightest particle in the final state, so that in our case we assume the cross sections are proportional to the maximum momentum that the kaon can have. We found it interesting to note that qualitative agreement with the data can already be obtained with two highly oversimplified models.

In the first we assumed a single step mechanism in which there is only a single nucleon-nucleon interaction between the projectile proton (or nucleon when nuclear projectiles are involved) and a nucleon within the target nucleus. The nucleons in the nuclei are assumed to have an exponential Fermi momentum distribution with a slope of 90 MeV. The results are shown in Figs. 17 and 18. One overall normalization was chosen to best fit the data. It is known from inclusive proton spectra in p-nucleus backward scattering that the same exponential distribution also gives a good fit to the data.[39-41] This distribution can be considered as an effective single-particle momentum distribution, which includes short-range correlations and final-state interactions.[42] The conclusion here is that the kaon spectra are already explained quite well by a single step mechanism with an effective momentum distribution which is the same as the

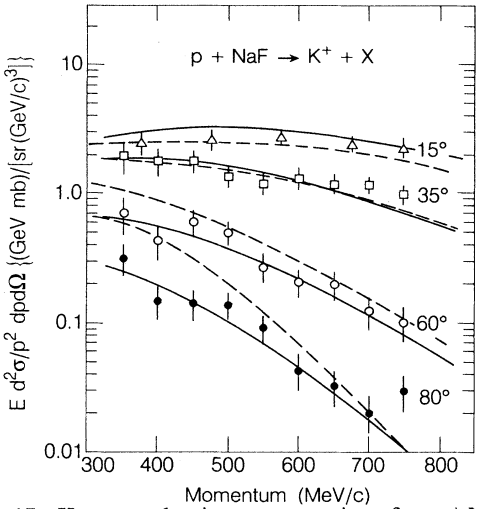

FIG. 17. Kaon production cross sections for $p+$NaF. The full curve shows the fits using a single nucleon-nucleon interaction with an exponential Fermi momentum distribution characterized by $f(P)=e^{-P/P_0}$ with $P_0=90$ MeV/c. The dashed curve shows the fits using the multinucleon cluster model, where the number of nucleons per cluster is given by Poisson statistics with $\langle n \rangle = 1$.

one used to explain backward proton emission from $p+A$ collisions.

We were also able to fit the data quite well with a very simple cluster model. Here we assumed collisions between two clusters containing n_P nucleons in the projectile cluster and n_T nucleons in the target cluster. The number of nucleons in each cluster was given by Poisson statistics; i.e., we calculated the statistical probability of finding n nucleons in a fixed volume, assuming no correlations and no interactions between them. The Fermi momentum of each cluster was determined by allowing each of the nucleons within the cluster to have a normal Fermi distribution given by a sharp radius of 270 MeV/c. In Figs. 17 and 18 we show the fits obtained to the $p+$NaF and Ne+NaF data using a Poisson distribution of nucleons in each cluster containing one nucleon on the average ($\langle n \rangle = 1$). Here, too, one overall normalization was chosen to fit the data. Similar fits to the $p+$Pb and Ne+Pb data are not as good, probably because rescattering corrections are not included. It is worth noting that in a Poisson distribution with $\langle n \rangle = 1$ the probability of finding two or more nucleons in the cluster, relative to that for finding only one is 72%. It is collisions between the multinucleon clusters that provides the energy for the highest-energy kaons.

By now a number of detailed intranuclear cascade calculations have been published.[5–16] In the case of kaon production the processes considered by the authors of these papers are (1) direct kaon production in reactions of the type $NN \rightarrow YNK$, (2) scattering of nucleons before (and after) kaon production, (3) production of an energetic pion which can subsequently react with another nucleon to produce a kaon, (4) $NN \rightarrow (N^*)N$ followed by $(N^*)N \rightarrow NYK$, where (N^*) is one of the nucleon isobars; e.g., Δ, and (5) scattering of the produced kaon on one or more of the available nucleons; i.e., a final-state interac-

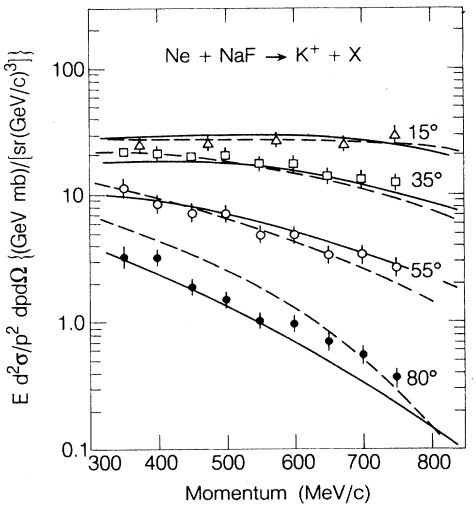

FIG. 18. Kaon production cross sections for Ne+NaF collisions. The full curve shows the fits using a single nucleon-nucleon interaction. The same Fermi distribution was assumed for both projectile and target nucleons. Relative positions of the cross sections are predicted by the model, but the overall normalization was chosen to fit the data. The dashed curve shows the fits using the multinucleon cluster model where the number of nucleons per cluster is given by Poisson statistics with $\langle n \rangle = 1$. Relative positions of the cross sections are predicted by the model, but the overall normalization was chosen to fit the data.

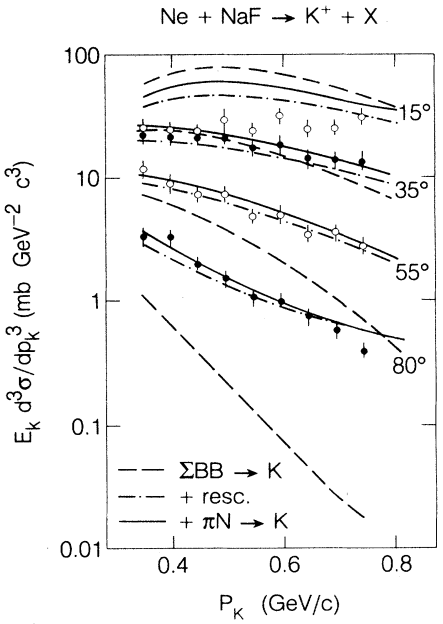

FIG. 19. Invariant K^+ production cross sections for several angles, compared to cascade model calculations of Ref. 9. The long dashed give the contribution to the primordial cross section coming from the baryon-baryon collisions. The dash and dotted curve is obtained by a rescattering correction to the first quantity. The full curve is finally obtained after addition of the πN contributions (without rescattering correction).

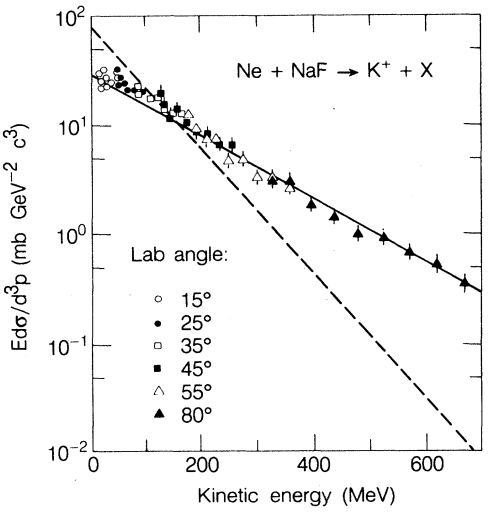

FIG. 20. Lorentz invariant kaon production cross section vs kinetic energy in the NN c.m. system at 2.1 GeV/nucleon compared to a cascade calculation using elementary cross sections given in Ref. 13. The dashed line shows the spectrum obtained in the earlier calculation of Randrup and Ko (Refs. 5 and 6).

tion of the K^+. Examples of the fits are shown in Figs. 19 and 20. In Fig. 19 we show the results of Cugnon and Lombard.[9] The long dashes give the contribution to the primordial cross section coming from baryon-baryon collisions. The dash-dotted curves are obtained by including rescattering of kaons. The full curves are obtained by adding the πN contribution (but do not include kaon rescattering). The fit obtained by Zwermann[13] is shown in Fig. 20. He parametrized the basic $NN \rightarrow YNK$ reaction by using phase-space considerations. No rescattering corrections are included in this work. The difference between these two calculations is attributed to the use of different basic $NN \rightarrow YNK$ cross sections. We refer the interested reader to the original publications for further details.[9,13]

B. Macroscopic models

Thermodynamic models assume that the region of overlap between colliding nuclei becomes completely thermalized during the collision. The momentum of the various particle types depend on the temperature of the system. These models contain a free parameter which is related to the freeze-out density. Early calculations[18] overestimated the K^+ yield by a factor of about 20, mainly because strangeness conservation was not properly included. More recent calculations[19–27] have remedied this problem, and agreement with experiment is thereby greatly improved. The calculations are now about a factor of 1.5 times higher than the data. This excess has been attributed to the breakdown of the assumption that the energy of the colliding particles is completely thermalized. Figure 21 shows a comparison between a thermal model,[26,27,32] a cascade model,[15] and the experimental points for the Ne+NaF$\rightarrow K^+$ reaction at 2.1 GeV/nucleon.[1] Both models reproduce the general trend of the data, although the cascade calculation is in better quantitative agreement.

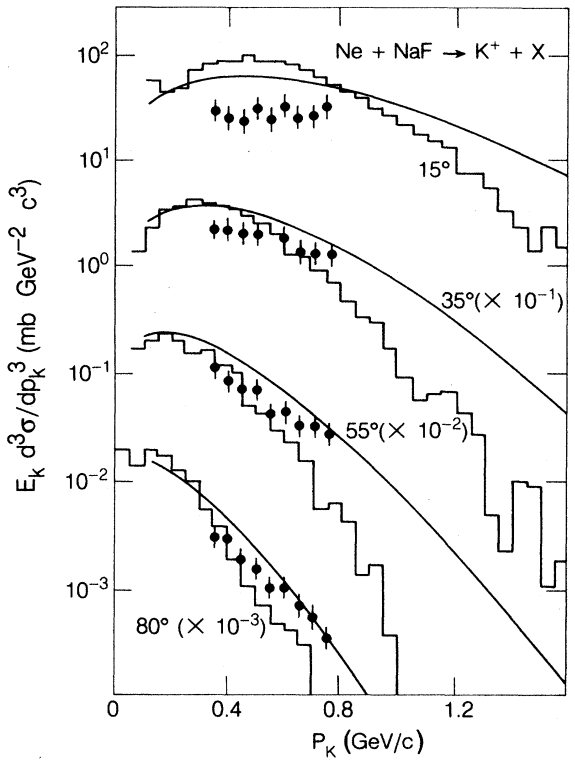

FIG. 21. Invariant spectrum of K^+ mesons from the Ne+NaF reaction at 2.1 GeV/nucleon. The histogram corresponds to the results of a cascade calculation (Ref. 15) and the curves to calculations with the firestreak model (Refs. 26, 27, and 32).

V. CONCLUSIONS

Our motivation for undertaking this experiment was to study hadronic interactions in heretofore unexplored territory. We hoped to exploit the unique properties of K^+ mesons—their strangeness and their relatively low-interaction cross sections—as a probe of nuclear interaction dynamics at high energies. We wanted to take advantage of their long mean free path to suppress secondary interactions and thereby to get more direct information about the early stages of the production process. Perhaps most of all we wanted to know whether or not kaon production in nucleus-nucleus collisions involved any interesting new phenomena, or if the measured cross sections could be explained on the basis of existing (standard) mechanisms.

Our results produced no great surprises. The mechanism for kaon production by nuclei seems to be quite similar to that in nucleon-nucleon collisions. To be sure there are kinematic differences. There is extra energy available when nuclei collide (as contrasted with the p-p case) some of which goes to the produced kaon, resulting in exponentially falling momentum distributions. The slope of the exponential is slightly less steep in the nucleus-nucleus case than for p nucleus. As in the p-p case the dominant reaction is $NN \rightarrow YNK$. Qualitative fits to the data can be obtained with single scattering models, either by invoking exponentially falling Fermi

momentum distributions or by colliding small clusters of nucleons. Much more sophisticated intranuclear cascade calculations and thermodynamic models have been published, which are in reasonable agreement with our measurements. Quarks, compressional effects, and/or other nonstandard mechanisms are not needed at this stage to explain the results.

Since the completion of the experimental part of this work there have been further speculations about how kaons might signal new phenomena. Among the topics mentioned in these papers are (1) the role of quark cluster states,[43,44] (2) compressional effects,[45,46] (3) high Fermi momentum components,[16,17] (4) the quark-gluon plasma,[47–50] (5) the time evolution of high-energy nuclear reactions,[51] (6) the nuclear equation of state,[52] and (7) subthreshold reaction mechanisms.[53–55] Although the results obtained here have shed little, if any, light on these issues, they seem to have at least stimulated considerable new theoretical and experimental activity.

As for the future it is clear that both the quality of the basic $NN \rightarrow YNK$ data, which is used as input in the theoretical model calculations, must be improved significantly,[13] and the kaon production measurements will have to be much more accurate and extensive before really meaningful tests of the models can be expected. They should cover a much wider range of bombarding energies, angles, and secondary momenta. More extensive studies of the mass dependence of the colliding nuclei have been suggested as a means of probing possible compressional effects.[53]

ACKNOWLEDGMENTS

We wish to thank the Bevalac operating crew for their support. The authors are grateful to O. Chamberlain for his continuous encouragement and to J. Randrup, J. Cugnon, H. Gyulassy, and J. Carroll for fruitful discussions. Special thanks go to Jeanne Miller for her essential help in preparing the manuscript. This work was supported by the U. S. Department of Energy under Contract No. DE-AC03-76SF00098. It was also supported by the Institute for Nuclear Studies–Lawrence Berkeley Laboratory Collaboration Program. One of us (R.M.L.) thanks the Centre National de la Recherche Scientifique for its support.

---

*Present address: Department of Physics, Rutgers University, New Brunswick, NJ 08903.

†Present address: Département de Physique Nucléaire à Moyennes Energies, Centre d'Etudes Nucléaires de Saclay, F-91191 Gif-sur-Yvette, France.

‡Present address: Institut für Theoretische Physik, Freie Universität Berlin, 1000 Berlin 33, Germany.

§Present address: Nevis Laboratories, P.O. Box 137, Irvington-on-Hudson, NY 10533.

**Also at Department of Physics, University of California, Berkeley, CA 94720.

††Present address: RIKEN, Institute of Physical and Chemical Research, 2-1 Hirosawa, Wako, Saitama 351-01, Japan.

[1]S. Schnetzer *et al.*, Phys. Rev. Lett. **49**, 989 (1982); Proceedings of the International Conference on Nuclear Physics, Berkeley, 1980, Lawrence Berkley Laboratory Report No. 11118, 1980, Vol. 1, p. 619.

[2]S. Schnetzer *et al.*, Proceedings of the High Energy Interaction and Properties of Dense Nuclear Matter, Hakoni, 1980 (unpublished), Vol. 1, p. 439.

[3]S. Nagamiya, Phys. Rev. Lett. **49**, 1383 (1982); in Proceedings of the High Energy Nuclear Physics Sixth Balaton Conference on Nuclear Physics, Balatonfured, 1983 edited by J. Erö (unpublished), p. 329.

[4]S. Schnetzer, Ph.D. thesis, Lawrence Berkley Laboratory Report No. 12727, 1981 (unpublished).

[5]J. Randrup and M. Ko, Nucl. Phys. **A343**, 519 (1980).

[6]J. Randrup and C. M. Ko, Nucl. Phys. **A411**, 537 (1983).

[7]J. Randrup, Phys. Lett. **99B**, 9 (1981).

[8]J. Cugnon and R. M. Lombard, Phys. Lett. **134B**, 392 (1984).

[9]J. Cugnon and R. M. Lombard, Nucl. Phys. **A422**, 635 (1984).

[10]W. Zwermann *et al.*, Phys. Lett. **134B**, 397 (1984).

[11]W. Zwermann and B. Schürmann, Nucl. Phys. **A423**, 525 (1984).

[12]B. Schürmann and W. Zwermann, Proceedings of the 7th High Energy Heavy Ion Study, Gesellschaft für Schwerionenforschung Report No. GSI-85-10, 1985, p. 275.

[13]W. Zwermann, Mod. Phys. Lett. **A3**, 251 (1988).

[14]H. W. Barz and H. Iwe, Phys. Lett. **143B**, 55 (1984).

[15]K. K. Gudima and V. D. Toneev, Proceedings of the 7th International Symposium on Problems of High Energy Physics Dubna, 1984, Joint Institute for Nuclear Research Report p. 567.

[16]N. A. Tarasov, V. P. Koptev, and M. M. Nesterov, Pis'ma Zh. Eksp. Teor. Fiz. **43**, 217 (1986) [JETP Lett. **43**, 274 (1986)].

[17]N. K. Abrasimov *et al.*, Pis'ma Zh. Eksp. Teor. Fiz. **43**, 214 (1986) [JETP Lett. **43**, 270 (1986)].

[18]F. Asai, H. Sato, and M. Sano, Phys. Lett. **98B**, 19 (1981).

[19]F. Asai and M. Sano, Prog. Theor. Phys. **66**, 251 (1981).

[20]F. Asai, Nucl. Phys. **A365**, 519 (1981).

[21]C. M. Ko, Phys. Rev. C **23**, 2760 (1981); **29**, 2169 (1984).

[22]F. Asai, H. Bando, and M. Sano, Phys. Lett. **145B**, 19 (1984).

[23]T. Biro *et al.*, Phys. Rev. C **27**, 2695 (1983).

[24]H. W. Barz *et al.*, Z. Phys. A **311**, 311 (1983).

[25]T. S. Biro, B. Lukas, J. Zimanyi, and H. W. Barz, Nucl. Phys. **A386**, 617 (1982).

[26]K. K. Gudima and V. D. Toneev, in Proceedings of the High Energy Nuclear Physics 6th Balaton Conference on Nuclear Physics, Balatonfured, 1983, edited by J. Erö (unpublished), p. 423.

[27]K. K. Gudima and V. D. Toneev, Yad. Fiz. **42**, 645 (1985) [Sov. J. Nucl. Phys. **42**, 409 (1985)].

[28]N. K. Abrasimov *et al.*, Leningrad Institute of Nuclear Physics Report 704, 1981; Leningrad Institute of Nuclear Physics Report 1146, 1985; Pis'ma Zh. Eksp. Teor. Fiz. **36**, 211 (1982) [JETP Lett. **36**, 261 (1982)].

[29]N. K. Abrasimov *et al.*, in *Book of Abstracts*, edited by F. Gutmer, B. Povh, and G. Zu Putlich (Springer-Verlag, Berlin, 1984), Vol. 2, p. I-6.

[30]A. A. Kuznetsov, Joint Institute for Nuclear Research Report E1-82-660, 1982.

[31]A. B. Kurepin *et al.*, Pis'ma Zh. Eksp. Teor. Fiz. **47**, 16 (1988)

[JETP Lett. **47**, 17 (1988)]; Proceedings of the High Energy Physics Problems, Dubna, 1986 (unpublished), Vol. 1, p. 273.
[32]V. D. Toneev *et al.*, Fiz. Elem. Chastits At. Yadra **17**, 1093 (1986) [Sov. J. Part. Nucl. **17**, 485 (1986)].
[33]S. Nagamiya *et al.*, Phys. Rev. C **24**, 971 (1981).
[34]Y. Miake *et al.*, Phys. Rev. C **31**, 2168 (1985).
[35]S. Nagamiya *et al.*, Phys. Rev. Lett. **48**, 1780 (1982); S. Nagamiya, Nucl. Phys. **A418**, 239 (1984).
[36]X. X. Bai *et al.*, Proceedings of the 6th High Energy Heavy Ion Study, 2nd Workshop on Anomalons, Berkeley, 1983 (unpublished), p. 255.
[37]O. Benary, L. R. Price, and G. Alexander, Lawrence Berkeley Laboratory Report UCRL-20000NN, 1970.
[38]W. J. Hogan, P. A. Piroue, and A. J. S. Smith, Phys. Rev. C **166**, 1472 (1968).
[39]S. Frankel *et al.*, Phys. Rev. Lett. **36**, 642 (1976).
[40]S. Frankel, Phys. Rev. Lett. **38**, 1338 (1977).
[41]S. Frankel *et al.*, Phys. Rev. C **18**, 1375 (1978).
[42]R. D. Amado and R. M. Woloshyn, Phys. Rev. Lett. **36**, 1435 (1976).
[43]B. Z. Kopeliovich and F. Niedermayer, Phys. Rev. C **33**, 2070 (1986).
[44]B. Z. Kopeliovich and F. Niedermyer, Yad. Fiz. **44**, 57 (1986) [Sov. J. Nucl. Phys. **44**, 333 (1986)]; Joint Institute for Nuclear Research Report P2-85-66, 1985.
[45]B. Schürmann and W. Zermann, Phys. Lett. B **183**, 31 (1987).
[46]J. Aichelin *et al.*, Phys. Rev. Lett. **58**, 1926 (1987).
[47]J. Rafelski and B. Muller, Phys. Rev. Lett. **48**, 1066 (1982).
[48]N. Glendenning and J. Rafelsky, Phys. Rev. C **31**, 823 (1985).
[49]P. Koch, B. Muller, and J. Rafelsky , Phys. Rep. **142**, 167 (1986).
[50]K. S. Lee and M. J. Rhoades-Brown, Phys. Rev. C **37**, 1463 (1988).
[51]K. K. Gudima *et al.*, Nucl. Phys. **A467**, 759 (1987).
[52]J. Aichelin and C. M. Ko, Phys. Rev. Lett. **55**, 2661 (1985).
[53]B. Schürmann and W. Zermann, Mod. Phys. Lett. **A3**, 1441 (1988).
[54]T. R. Halemane and A. Z. Mekjian, Phys. Rev. C **25**, 2398 (1982).
[55]Che Ming Ko and Linhua Xia, Phys. Rev. C **38**, 179 (1988).